

## Electronic Supplementary Information (ESI)

### **Superior Wear Resistance and Low Friction in Hybrid Ultrathin Silicon Nitride/Carbon Films: Synergy of Interfacial Chemistry and Carbon Microstructure**

Reuben J. Yeo,<sup>a</sup> Neeraj Dwivedi,<sup>a</sup> Lu Zhang,<sup>b</sup> Zheng Zhang,<sup>c</sup> Christina Y. H. Lim,<sup>d</sup> Sudhiranjan Tripathy,<sup>c</sup> and Charanjit S. Bhatia\*<sup>a</sup>

*<sup>a</sup> Department of Electrical and Computer Engineering, National University of Singapore, Singapore 117583*

*E-mail: [elebcs@nus.edu.sg](mailto:elebcs@nus.edu.sg)*

*<sup>b</sup> Institute of Microelectronics, A\*STAR (Agency for Science, Technology and Research), 11 Science Park Drive, Singapore 117685*

*<sup>c</sup> Institute of Materials Research and Engineering, A\*STAR (Agency for Science, Technology and Research), 2 Fusionopolis Way, Singapore 138634*

*<sup>d</sup> Department of Mechanical Engineering, National University of Singapore, Singapore 117575*

## Content of the ESI

- S1. List of samples and their descriptions
- S2. Sample preparation for high resolution transmission electron microscopy (HRTEM) cross-section imaging
- S3. Multiwavelength Raman spectra analyses of the films
- S4. XPS C 1s spectra analyses of the as-grown films
- S5. Wear track analysis by micro-Raman spectroscopy for single-component sputter-grown carbon film (7CP)

### S1. List of samples and their descriptions

**Table S1** List of samples used in this work, with the descriptions of their respective film structure, fabrication process and thickness. All substrate cleaning and film depositions were performed *in-situ* in an ultra-high vacuum chamber.

| Samples                    | Description of film structure and its fabrication process   | Thickness of SiN <sub>x</sub> (nm) | Thickness of carbon (nm) | Total measured film thickness (nm) |
|----------------------------|---|------------------------------------|--------------------------|------------------------------------|
| <b>7CF90</b>               | Single-component carbon film structure of ~7 nm. Ar <sup>+</sup> plasma cleaning of the substrate was performed before deposition of the carbon film by FCVA with C <sup>+</sup> ions at 90 eV.   | -                                  | ~7                       | 7.1 ± 0.1                          |
| <b>T<sub>A</sub>/7CF90</b> | Single-component carbon film structure of ~8.5 nm. Ar <sup>+</sup> plasma cleaning of the substrate was first performed before surface treatment process T <sub>A</sub> was carried out by FCVA with high energy C <sup>+</sup> ions at 350 eV. Finally, the carbon film was deposited by FCVA with C <sup>+</sup> ions at 90 eV. | -                                  | ~8.5                     | 8.8 ± 0.2                          |

|                                 |   |    |    |           |
|---------------------------------|---|----|----|-----------|
| <b>3SiN/4CF90</b>               | Hybrid SiN <sub>x</sub> /C film structure of ~7 nm. Ar <sup>+</sup> plasma cleaning of the substrate was first performed. SiN <sub>x</sub> was then deposited by RF sputtering. Finally, carbon was deposited by FCVA with C <sup>+</sup> ions at 90 eV.  | ~3 | ~4 | 7.2 ± 0.2 |
| <b>3SiN/T<sub>B</sub>/4CF90</b> | Hybrid SiN <sub>x</sub> /C film structure of ~8 nm. Ar <sup>+</sup> plasma cleaning of the substrate was first performed. SiN <sub>x</sub> was then deposited by RF sputtering. Next, surface treatment process T <sub>B</sub> was carried out by FCVA with high energy C <sup>+</sup> ions at 350 eV. Finally, carbon was deposited by FCVA with C <sup>+</sup> ions at 90 eV. | ~3 | ~5 | 7.8 ± 0.2 |
| <b>7CP</b>                      | Single-component carbon film structure of ~7 nm. Ar <sup>+</sup> plasma cleaning of the substrate was performed before deposition of the carbon film by pulsed DC sputtering.   | -  | ~7 | 6.9 ± 0.3 |
| <b>3SiN/4CP</b>                 | Hybrid SiN <sub>x</sub> /C film structure of ~7 nm. Ar <sup>+</sup> plasma cleaning of the substrate was first performed. SiN <sub>x</sub> was then deposited by RF sputtering. Finally, carbon was deposited by pulsed DC sputtering.  | ~3 | ~4 | 7.5 ± 0.2 |
| <b>7SiN</b>                     | Single-component SiN <sub>x</sub> film structure of ~7 nm. Ar <sup>+</sup> plasma cleaning of the substrate was performed before deposition of the SiN <sub>x</sub> film by RF sputtering.  | ~7 | -  |           |

## **S2. Sample preparation for high resolution transmission electron microscopy (HRTEM) cross-section imaging**

Films deposited on Si substrates were used for cross-section imaging by high resolution transmission electron microscopy (HRTEM). Sample preparation for HRTEM cross-section imaging was performed according to the following steps:

- 1) Before overcoat deposition, a capping layer of Ta was deposited on the Si substrates to avoid the contribution of native silicon oxide ( $\text{SiO}_x$ ) to the thickness measurement, since it exhibits a similar contrast to  $\text{SiN}_x$  and carbon in HRTEM imaging.
- 2) After carbon or  $\text{SiN}_x/\text{C}$  film deposition, a capping layer of Ta was deposited onto the overcoats. This layer helped in providing the contrast between the carbon layer/ $\text{SiN}_x$  layer and epoxy glue which was to be applied in the subsequent step.
- 3) After capping layer deposition, two pieces of samples were taken and then stuck together face-to-face with heat-curable epoxy glue.
- 4) Curing of the epoxy was performed by heating the glued specimen on a hot plate at  $\sim 120^\circ\text{C}$ .
- 5) Once the epoxy had cured, the specimen was mechanically polished down along the specimen edge to reduce its size to a suitable thickness level of about  $50\ \mu\text{m}$ .
- 6) The polished specimen was then cleaned with acetone and isopropyl alcohol solvents to remove any debris attached to the specimen as a result of polishing.
- 7) After washing, the specimen was transferred and attached to a Cu ring for mechanical support.
- 8) Finally, ion milling was carried out by directing  $\text{Ar}^+$  ions at a narrow angle (approximately  $3\text{-}5^\circ$ ) with respect to the specimen surface to create a hole in the middle of the specimen. Because of the narrow angle, the hole periphery would have a gentle gradient whereby the specimen thickness would be thin enough to be

electron transparent in HRTEM imaging. This hole would form at the interface where the two Si substrates were glued together.

The region of interest on for HRTEM cross-section imaging would therefore be the electron transparent areas created at the hole periphery of the specimen.

### S3. Multiwavelength Raman spectra analyses of the films

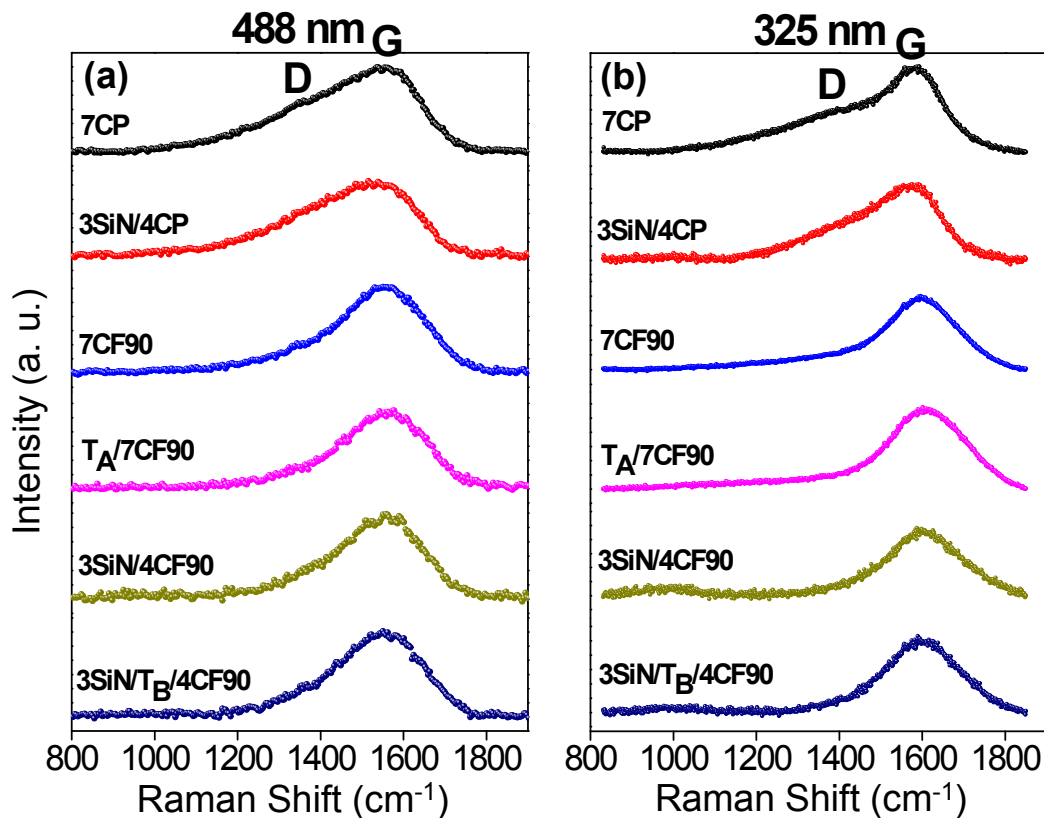


**Fig. S1** (a) Visible (488 nm) and (b) UV (325 nm) Raman spectra of the as-grown single-component and hybrid carbon-based films on AlTiC. The positions of the D and G peaks are indicated in the figure.

The visible and UV Raman spectra obtained for the as-grown carbon-based films are presented in Fig. S1. All the Raman spectra showed a band comprising the characteristic D and G peaks typically observed for amorphous carbon. On first observation, there is a noticeable difference in the spectral shapes of the films containing sputter-grown carbon and the films containing FCVA-grown carbon in both the visible and UV spectra, because of a

higher D peak intensity (at  $\sim 1300\text{--}1400\text{ cm}^{-1}$ ) observed for the sputter-grown carbon films. Peak fitting was carried out on the spectra, with the D peaks fitted using a Lorentzian function and the G peaks fitted using a Breit-Wagner-Fano (BWF) function (not shown in the Raman spectra). Consequently, the G peak position ( $G_{Pos}$ ) for each spectrum could be determined. From the  $G_{Pos}$  of the visible and UV Raman spectra, the G peak dispersion ( $G_{dis}$ ) was calculated for each film using the formula:<sup>1</sup>

$$G_{dis} = \frac{(G_{Pos}(UV)) - (G_{Pos}(Vis))}{\Delta\lambda}$$

where  $G_{Pos}(UV)$  is the G peak position in the UV Raman spectrum,  $G_{Pos}(Vis)$  is the G peak position in the visible Raman spectrum, and  $\Delta\lambda$  is the difference in the excitation wavelengths (i.e.  $\Delta\lambda = 488\text{ nm} - 325\text{ nm} = 163\text{ nm}$ ). In addition, the ratio of the D peak intensity to the G peak intensity ( $I_D/I_G$  ratio) could be calculated for each spectrum. The  $G_{Pos}$ ,  $G_{dis}$ , and  $I_D/I_G$  ratios were used to analyze the carbon microstructures of the films and estimate the  $sp^3$  carbon ( $sp^3C$ ) bonding fraction for each film, based on the three-stage model proposed by Ferrari and Robertson.<sup>1,2</sup>

We also recorded the Raman spectra of the single-component sputter-grown and FCVA-grown carbon films at higher excitation wavelength of 785 nm (near IR) from a diode laser, to ensure a reliable determination of the trend of the  $sp^3$  content by micro-Raman spectroscopy. After performing standard fitting procedure, we measured the  $G_{Pos}(near\ IR)$  as well as the  $G_{dis}$  values using the combination of 325 nm and 785 nm wavelengths ( $\Delta\lambda = 785\text{ nm} - 325\text{ nm} = 460\text{ nm}$ ) for these samples, which are presented in Fig. S2. We also compared the  $G_{dis}$  measured at two different combinations of wavelengths, 325 nm–488 nm and 325 nm–785 nm, for these non-hydrogenated amorphous carbon films, Fig. S2c. We found that the  $G_{dis}$  values were always significantly higher in samples 7CF90 and T<sub>A</sub>/7CF90 than in sample 7CP, indicating that the FCVA-grown carbons possess much higher  $sp^3$  bonding than sputter-grown carbon. However, the difference in the  $G_{dis}$  values between

FCVA- and sputter-grown carbon was found to be relatively lower when the combination of 325 nm and 488 nm wavelengths was used for the calculation than when using the combination of 325 nm and 785 nm excitation wavelengths. This is due to fact that the 325 nm and 488 nm wavelengths are relatively closer together as compared to the 325 nm and 785 nm wavelengths. Further details on the Raman analyses of these samples can be found in a recent publication.<sup>3</sup>

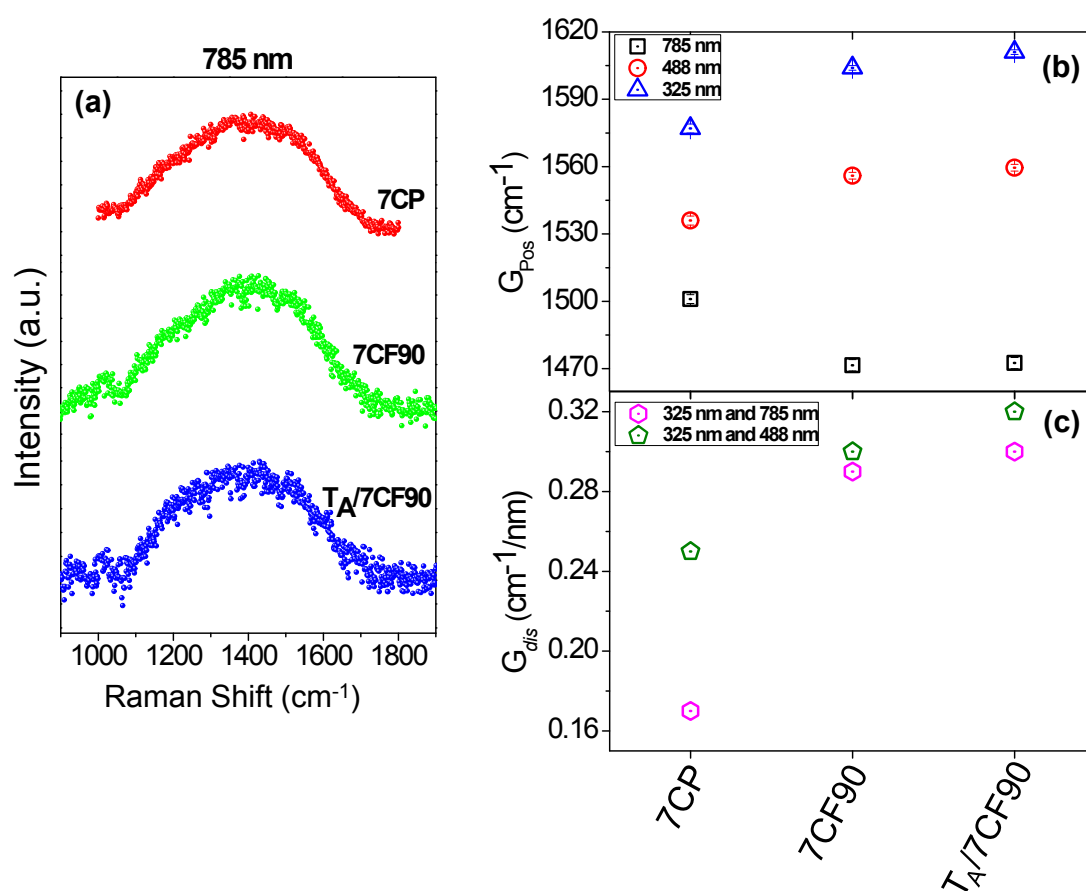


**Fig. S2** Raman measurements on samples 7CP, 7CF90 and TA/7CF90 at excitation wavelength of 785 nm. (a) Representative Raman spectra of each sample recorded at 785 nm; (b) variation of  $G_{Pos}$  at excitation wavelengths of 325 nm, 488 nm and 785 nm; (c)  $G_{dis}$  values calculated for the combinations of 325 nm and 785 nm wavelengths, and 325 nm and 488 nm wavelengths.

#### S4. XPS C 1s spectra analyses of the as-grown films

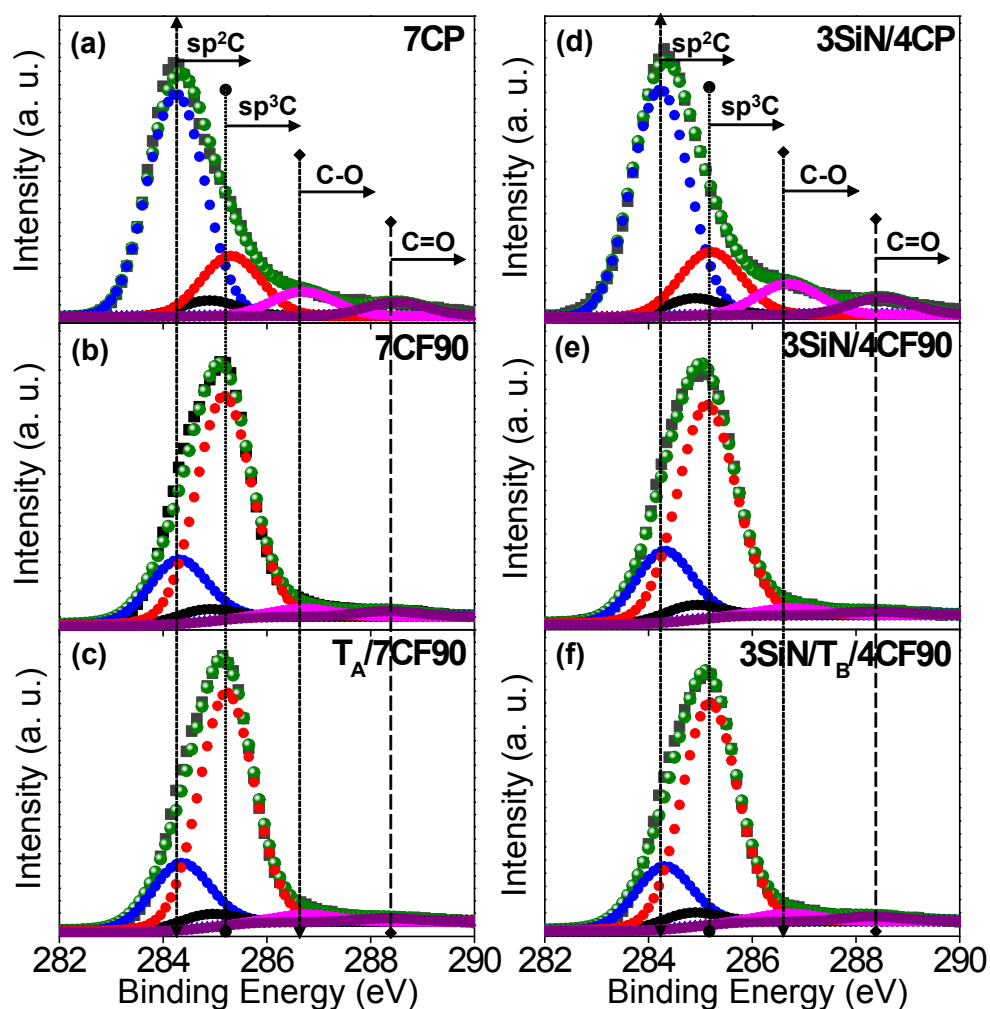


**Fig. S3** (a)–(f) Deconvoluted XPS C 1s spectra of the as-grown carbon-based films showing the constituent bonding peaks corresponding to  $sp^2C$ ,  $sp^3C$ , C–O, and C=O. The adventitious carbon peak is not labeled, but can be observed as a small black-colored peak situated between the  $sp^2C$  and  $sp^3C$  peaks.

C 1s XPS spectra obtained on the as-grown films (0 s sputter etching) were deconvoluted to show four constituent peaks corresponding to  $sp^2C$ ,  $sp^3C$ , C–O, and C=O bonding (Fig. S3). In addition, an adventitious carbon (AC) peak (not labeled in the spectra) was included as one of the peaks during deconvolution, in consideration of the likely presence of adventitious carbon on the surface from environmental contamination.<sup>4</sup> The peak positions and full width half maxima (FWHM) of all the peaks were maintained as similar for all films.

From the deconvoluted spectra, it can be clearly distinguished that the  $sp^2C$ , C–O and C=O bonding fractions for the sputter-grown films were substantially higher than those in the FCVA-grown films, whereas the  $sp^3C$  fraction was observed to be higher in the FCVA-grown films. Nevertheless, we proceeded to estimate the  $sp^3C$  bonding from the XPS spectra by applying an area ratio method to calculate the relative areas of each constituent peak (and hence determine the bonding fraction). The amount of  $sp^3C$  bonding is given by:

$$\%sp^3C = \frac{A(sp^3C)}{\sum A(sp^3C + sp^2C + C-O + C=O + AC)} \times 100\%$$

where  $A(sp^3C)$  represents the area of the  $sp^3C$  peak and  $\sum A(sp^3C + sp^2C + C-O + C=O + AC)$  is the sum of the areas under the peaks  $sp^3C$ ,  $sp^2C$ , C–O, C=O, and AC.

Further details on the constituent peak positions, FWHM and  $sp^3C$  bonding calculations can be found in a recent publication.<sup>3</sup>

### **S5. Wear track analysis by micro-Raman spectroscopy for single-component sputter-grown carbon film (7CP)**

From ball-on-disk micro-tribological measurements on the sputter-grown single-component carbon film (7CP), we found significant wear of the sample after the tribological tests, based on the increase in the COF during the wear test and visible wear track and debris/tribofilm transfer to the ball. We used micro-Raman spectroscopy to analyze the local carbon content outside the wear track and at three locations on the wear track. The Raman spectra are presented in Fig. S4. Based on the lower Raman signal intensity derived from the locations on the wear track than outside the wear track (unworn carbon film), the results suggested the removal of a large amount of amorphous carbon in the wear track.

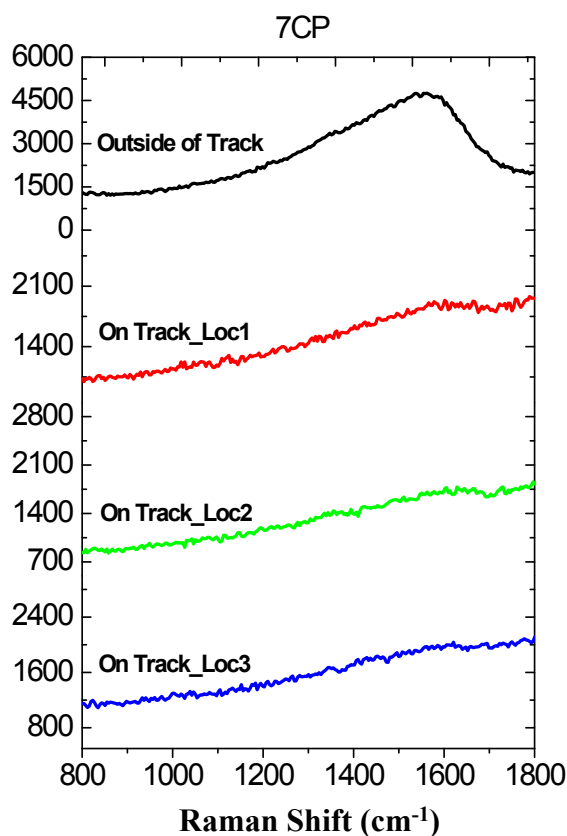


**Fig. S4** Raman spectra of sample 7CP recorded outside of the wear track region as well as on various locations of the wear track.

## References

- 1 A. C. Ferrari and J. Robertson, *Phil. Trans. R. Soc. Lond. A*, 2004, **362**, 2477–2512.
- 2 A. C. Ferrari and J. Robertson, *Phys. Rev. B*, 2000, **61**, 14095–14107.
- 3 N. Dwivedi, R. J. Yeo, Z. Zhang, C. Dhand, S. Tripathy and C. S. Bhatia, *Carbon*, 2017, **115**, 701–719.
- 4 N. Dwivedi, R. J. Yeo, L. J. K. Yak, N. Satyanarayana, C. Dhand, T. N. Bhat, Z. Zhang, S. Tripathy and C. S. Bhatia, *ACS Appl. Mater. Interfaces*, 2016, **8**, 17606–17621.